



**AFRL-RX-WP-TP-2009-4125**

**DEVELOPMENT OF METHODS FOR THE  
QUANTIFICATION OF MICROSTRUCTURAL FEATURES  
IN  $\alpha+\beta$  PROCESSED  $\alpha/\beta$  TITANIUM ALLOYS (PREPRINT)**

**P.C. Collins, B. Welk, T. Searles, J. Tiley, J.C. Russ, and H.L. Fraser**

**University of North Texas**

**MARCH 2009**

**Approved for public release; distribution unlimited.**

*See additional restrictions described on inside pages*

**STINFO COPY**

**AIR FORCE RESEARCH LABORATORY  
MATERIALS AND MANUFACTURING DIRECTORATE  
WRIGHT-PATTERSON AIR FORCE BASE, OH 45433-7750  
AIR FORCE MATERIEL COMMAND  
UNITED STATES AIR FORCE**

<b>REPORT DOCUMENTATION PAGE</b>				<i>Form Approved</i> OMB No. 0704-0188	
<p>The public reporting burden for this collection of information is estimated to average 1 hour per response, including the time for reviewing instructions, searching existing data sources, gathering and maintaining the data needed, and completing and reviewing the collection of information. Send comments regarding this burden estimate or any other aspect of this collection of information, including suggestions for reducing this burden, to Department of Defense, Washington Headquarters Services, Directorate for Information Operations and Reports (0704-0188), 1215 Jefferson Davis Highway, Suite 1204, Arlington, VA 22202-4302. Respondents should be aware that notwithstanding any other provision of law, no person shall be subject to any penalty for failing to comply with a collection of information if it does not display a currently valid OMB control number. <b>PLEASE DO NOT RETURN YOUR FORM TO THE ABOVE ADDRESS.</b></p>					
<b>1. REPORT DATE (DD-MM-YY)</b> March 2009		<b>2. REPORT TYPE</b> Journal Article Preprint		<b>3. DATES COVERED (From - To)</b>	
<b>4. TITLE AND SUBTITLE</b> DEVELOPMENT OF METHODS FOR THE QUANTIFICATION OF MICROSTRUCTURAL FEATURES IN $\alpha+\beta$ PROCESSED $\alpha/\beta$ TITANIUM ALLOYS (PREPRINT)				<b>5a. CONTRACT NUMBER</b> FA8650-08-C-5226	
				<b>5b. GRANT NUMBER</b>	
				<b>5c. PROGRAM ELEMENT NUMBER</b> 62102F	
<b>6. AUTHOR(S)</b> P.C. Collins, B. Welk, and H.L. Fraser (The Ohio State University) T. Searles (Rolls Royce Company) J. Tiley (AFRL/RXLMD) J.C. Russ (North Carolina State University)				<b>5d. PROJECT NUMBER</b> 4349	
				<b>5e. TASK NUMBER</b> 20	
				<b>5f. WORK UNIT NUMBER</b> LM114100	
<b>7. PERFORMING ORGANIZATION NAME(S) AND ADDRESS(ES)</b>				<b>8. PERFORMING ORGANIZATION REPORT NUMBER</b>	
The Ohio State University 2041 College Road Columbus, OH		Metals Branch (AFRL/RXLMD) Metals, Ceramics, and NDE Division Materials and Manufacturing Directorate Wright-Patterson Air Force Base, OH 45433-7750 Air Force Materiel Command, United States Air Force			
----- Rolls Royce Company Indianapolis, IN		----- North Carolina State University Raleigh, NC			
<b>9. SPONSORING/MONITORING AGENCY NAME(S) AND ADDRESS(ES)</b>				<b>10. SPONSORING/MONITORING AGENCY ACRONYM(S)</b>	
Air Force Research Laboratory Materials and Manufacturing Directorate Wright-Patterson Air Force Base, OH 45433-7750 Air Force Materiel Command United States Air Force				AFRL/RXLMD	
				<b>11. SPONSORING/MONITORING AGENCY REPORT NUMBER(S)</b> AFRL-RX-WP-TP-2009-4125	
<b>12. DISTRIBUTION/AVAILABILITY STATEMENT</b> Approved for public release; distribution unlimited.					
<b>13. SUPPLEMENTARY NOTES</b> Journal article submitted to <i>Materials Science and Engineering</i> . PAO Case Number: 88 ABW-2009-0626; Clearance Date: 20 Feb 2009. The U.S. Government is joint author of this work and has the right to use, modify, reproduce, release, perform, display, or disclose the work.					
<b>14. ABSTRACT</b> A set of stereological procedures has been developed for the rigorous quantification of microstructural features resolvable using scanning electron microscopy in $\alpha+\beta$ processed $\alpha/\beta$ titanium alloys. This paper identifies the four microstructural features that most likely influence the mechanical properties in $\alpha+\beta$ processed titanium alloy, including: the size of the equiaxed alpha, the volume fraction of the equiaxed alpha, the volume fraction of total alpha, and the thickness of the Widmanstätten alpha laths. The details regarding the quantification methodologies are provided, as are the origins of the associated uncertainties.					
<b>15. SUBJECT TERMS</b> microstructural quantification, stereology, titanium					
<b>16. SECURITY CLASSIFICATION OF:</b>			<b>17. LIMITATION OF ABSTRACT:</b> SAR	<b>18. NUMBER OF PAGES</b> 26	<b>19a. NAME OF RESPONSIBLE PERSON (Monitor)</b> Jay Tiley <b>19b. TELEPHONE NUMBER (Include Area Code)</b> N/A
<b>a. REPORT</b> Unclassified	<b>b. ABSTRACT</b> Unclassified	<b>c. THIS PAGE</b> Unclassified			

# Development of methods for the quantification of microstructural features in $\alpha+\beta$ processed $\alpha/\beta$ titanium alloys

P.C. Collins<sup>a</sup>, B. Welk<sup>a</sup>, T. Searles<sup>b</sup>, J. Tiley<sup>c</sup>, J.C. Russ<sup>d</sup>, and H.L. Fraser<sup>a</sup>

<sup>a</sup> Center for the Accelerated Maturation of Materials, Department of Materials Science & Engineering, The Ohio State University, 2041 College Road, Columbus, Ohio, USA

<sup>b</sup> Rolls Royce Company, Indianapolis, IN

<sup>c</sup> Air Force Research Laboratory, Materials & Manufacturing Directorate, Wright - Patterson Air Force Base, Dayton, Ohio, USA

<sup>d</sup> North Carolina State University, Raleigh, NC, USA

Peter C. Collins, corresponding author. collins.457@osu.edu, (614) 292-4340

## Abstract

A set of stereological procedures has been developed for the rigorous quantification of microstructural features resolvable using scanning electron microscopy in  $\alpha+\beta$  processed  $\alpha/\beta$  titanium alloys. This paper identifies the four microstructural features that most likely influence the mechanical properties in  $\alpha+\beta$  processed titanium alloy, including: the size of the equiaxed alpha, the volume fraction of the equiaxed alpha, the volume fraction of total alpha, and the thickness of the Widmanstätten alpha laths. The details regarding the quantification methodologies are provided, as are the origins of the associated uncertainties.

**Keywords:** microstructural quantification, stereology, titanium

## 1. Introduction

The balance of properties, particularly the high strength, good ductility, and enhanced fracture toughness, of  $\alpha+\beta$ -processed Ti alloys is particularly attractive in many applications in the aerospace industry. It is claimed that these properties are dependent upon the microstructural features [1-5]. However, there does not exist a model which accurately predicts the mechanical properties of a microstructure given a set of microstructural variables. Indeed, the very best tools available establish whether a microstructural feature has a positive (+), negative (-), or neutral (0) influence on the mechanical properties of Ti alloys [5]. The absence of any physically based model is largely predicted by the complicated interdependencies that exist among the microstructural features. A solution to the complex problem of isolating and quantifying the magnitude of the functional dependencies of property on microstructure or processing involves the use of rules-based approaches. One such approach is neural networks based on Bayesian statistics (i.e., Bayesian Neural Networks) based on the work of D. MacKay [6-8]. This approach is particularly powerful in that the neural network is optimized without over-fitting for a particular problem. The fidelity of a solution (e.g., predicted property) provided by any rules-based approach is dictated by the quality and amount of the data used to train it. Hence, for the development of neural networks based on databases relating microstructures and mechanical properties, it is essential to develop

rigorous procedures for providing an accurate, quantified description of the microstructural features present in a digital micrograph.

Previously, the authors have presented such rigorous stereological tools in a newly developed computer imaging analysis toolkit for  $\beta$ -processed  $\alpha/\beta$  Ti-alloy type microstructures [9-11]. They have demonstrated the possibility of developing automated or semi-automated tools to determine average values of the complex microstructural features present in these alloys, such as the thickness of the Widmanstätten  $\alpha$ -laths, the colony scale factor, the prior  $\beta$  grain factor, and the volume fraction of Widmanstätten  $\alpha$ . The same authors later revisited the importance of determining the volume fraction of colony in a microstructure which contains both basketweave and colonies, and as a result, developed a microstructure-property neural network based model with a predictive accuracy of  $\pm 3\%$  of an experimentally measured property - a value that has *defined* the state-of-the-art modeling of properties for Ti-based alloys [12]. Indeed, the stereological procedures developed for  $\beta$ -processed  $\alpha/\beta$  Ti-alloy type microstructures has been demonstrated to have overcome many of the limitations of other manual procedures, such as user subjectivity [11].

The goal of this paper is to extend the original work to include a set of tools to describe quantitatively the microstructural features present in  $\alpha+\beta$  processed  $\alpha/\beta$  Ti-based alloys, such as Ti-6-4. While some of the features of the  $\alpha+\beta$ -processed microstructures are similar to those of the  $\beta$ -processed microstructures (e.g., Widmanstätten  $\alpha$ -laths described by an average thickness), others are quite different, as seen when comparing the  $\beta$ -processed microstructures (Fig. 1(a)) with the  $\alpha+\beta$ -processed microstructures (Fig. 1(b)). The most distinctive microstructural feature uniquely present in the  $\alpha+\beta$  processed material is equiaxed  $\alpha$  (often called globular  $\alpha$  or primary  $\alpha$ ). Such equiaxed  $\alpha$  forms during the thermomechanical processing and subsequent aging in the  $\alpha+\beta$  phase field, and is reported to play a crucial role in dictating the mechanical properties for a given microstructure. Indeed, to a first approximation, the presence of such  $\alpha$  has been argued to lead to enhanced fatigue properties due to its ability to blunt or arrest cracks [4].

Based upon both the previous work describing  $\beta$ -processed Ti alloys (for those microstructural features common to both  $\beta$ -processed and  $\alpha+\beta$ -processed Ti alloys) and the current qualitative understanding of deformation mechanisms in  $\alpha+\beta$ -processed  $\alpha/\beta$  Ti alloys such as Ti-6Al-4V, the microstructural features that have been identified for quantification are:

1. mean equiaxed- $\alpha$  size
2. volume fraction equiaxed- $\alpha$
3. volume fraction total  $\alpha$  and,
4. thickness of Widmanstätten  $\alpha$ -laths in transformed  $\beta$ .

The current paper describes the development of the stereological procedures for these four microstructural features. Although the estimation of the thickness of the Widmanstätten  $\alpha$ -laths has been described in previous work, it is included here for completeness, with an additional discussion regarding the limitations to the original derivation.

## 2. Experimental procedures

A total of 34 samples (2 samples from 17 unique thermal histories) from one industrially processed heat, and hence of a uniform composition, were thermomechanically processed in the  $\alpha+\beta$  phase field. The composition, nominally Ti-6Al-4V, was determined to be Ti-6.5Al-4.0V-0.15Fe-0.19O using inert gas atomization. The billets were forged using industrial practices at 968°C to two strain levels ( $\epsilon = 40\%$  & 80%), sectioned into samples, and subsequently subjected to combinations of different solution temperatures ( $> 968^\circ\text{C}$ ), cooling rates (0.37°C/sec to 3.7°C/sec), aging temperatures (593°C to 704°C) and aging times (2 to 8 hours). Table 1 provides additional details regarding the intermediate thermomechanical processing conditions.

The samples were subjected to room temperature tensile tests. Following the tensile tests, an undeformed section of the grip from each sample was sectioned for metallographic preparation. Following traditional metallographic techniques, the samples were characterized using a FEI/Philips Sirion scanning electron microscope (SEM) operating in backscattered mode at 15 kV with a resolution of approximately 2.0 nm. Each image had a resolution of 3872 x 2904 pixels and a depth of 8 bit. The resolution afforded using the SEM, especially when compared with other available techniques (e.g., optical micrographs), is of paramount importance to provide the highest fidelity quantified microstructural data to the neural networks. The specimens were imaged at four random locations avoiding overlap and edge effects. These four micrographs were quantified using the developed stereological techniques (described below) to improve sampling statistics and to provide an overall representation of the specimens' microstructures. The micrographs were saved using the uncompressed tagged image file format (\*.tiff).

The backscattered electron micrograph in Fig. 2(a) clearly shows the two distinct phases, namely the  $\alpha$  (hcp) and  $\beta$  (bcc) phases, which are most easily identified by their relative contrasts – a result of their respective average atomic mass. The  $\alpha$  phase, stabilized by elements with a low atomic number (e.g., Al and O) appears darker relative to the  $\beta$  phase, stabilized by the heavier elements (e.g., V and Fe). In addition to the Z-contrast, there is also channeling contrast that is present, and is most easily observed within the  $\alpha$  phase (*see fig. 2a*). Figs. 2 (b-c) are histograms of the contrast variation in the alpha phase with and without contrast variations due to channeling contrast, respectively, while Fig. 2 (d) shows the complete histogram for the microstructure in Fig. 2 (a). Given the nearly continual contrast variation that is observed in these microstructures, and the fact that the stereological procedures are developed based on a clear distinction between the two phases, it is essential to threshold the micrographs to precisely delineate the two phases. Therefore, using a semi-automated thresholding procedure, including a Gaussian operation to reduce the channeling contrast present in the  $\alpha$ -phase, each micrograph was converted to a binary image (*see Fig. 2 (e)*).

Additional preprocessing steps are required for each of the stereology procedures which follow. Of paramount importance is the proper identification and selection of the equiaxed  $\alpha$ . Such a task presents difficulties as the equiaxed  $\alpha$  that is present in these alloys can exhibit a significant range in size, depending on the thermomechanical processing, as shown by some of the extreme variations in size and volume fraction of microstructural features that can occur in Figs. 3(a-c). These three figures correspond to

samples forged within the  $\alpha+\beta$  two phase field at 968°C to either 40% strain (Figs. 3(a,c)) or 80% strain (Fig. 3(b)). Following the forging, the sample corresponding to Fig. 3(a) was solutionized in the two phase field at 985°C, cooled at 3.7°C, and aged at 704°C for two hours. The sample corresponding to Fig. 3(b) was solutionized in the two phase field at 977°C, cooled at 0.37°C, and aged at 593°C for eight hours. The sample corresponding to Fig. 3(c) was solutionized in the two phase field at 968°C, cooled at 0.37°C, and aged at 704°C for two hours. The microstructural variation that is illustrated in Figs. 3(a-c) presents a significant challenge to the development of an automated routine for the identification and isolation of the equiaxed  $\alpha$ . Currently, the most robust, automated routine will either miss small equiaxed  $\alpha$  particles or identify as equiaxed  $\alpha$  regions that would otherwise be considered to be grain boundary  $\alpha$  or a large Widmanstätten  $\alpha$ -lath. An example of this misidentification is shown in Fig. 4 (b) for the representative micrograph shown in Fig. 4(a). Therefore, additional manual selection of equiaxed  $\alpha$  is required to define all equiaxed  $\alpha$  particles (Fig. 4(c)) and then separate the individual particles (Fig. 4(d)). Work is currently underway to develop a fully automated method for identification of equiaxed  $\alpha$  in SEM micrographs.

Following these two initial preprocessing procedures, the stereological procedures described below can be performed. The stereological procedures were all performed on desktop computers running Adobe Photoshop 7.0 or CS2 with Fovea Pro®, a commercial plug-in set available from Reindeer Graphics, Asheville, NC. Where possible, the following procedures were fully automated using the action and droplet functions available in Adobe Photoshop.

## 2.1 Stereological Procedures for $\alpha+\beta$ processed Ti-Alloys

### 2.1.1 Mean size of equiaxed $\alpha$

In addition to the preprocessing of the images to select the equiaxed  $\alpha$ , it was necessary to separate the individual particles from clusters of the equiaxed phase for the calculation of its mean size (*see Figs. 4(c-d)*). This additional step is required given that a cluster of equiaxed  $\alpha$  particles may be composed of regions of different orientations, as evidenced by the variation in channeling contrast, or have internal, high-angle interfaces. Once this manual step is completed, the mean linear intercept was determined using a Fovea Pro™ plug-in. This plug-in superimposes a grid of parallel lines on a binary image, rotates the grid by successive 10° increments to collect measurements in multiple directions (*see Fig. 5(b)*), and records both the mean linear intercept and the mean of the inverse of the intercepts (*mean inverse intercept*), as well as a graphical measure of the measurement anisotropy present within a particular micrograph. It is important to make a distinction between the mean linear intercept which is used to determine the mean size of the equiaxed  $\alpha$ , and the mean inverse intercept, which is used for estimating the true thickness of Widmanstätten  $\alpha$ -laths. The mean linear intercept provides a direct estimation, with a shape factor where appropriate, for *geometrically simple* shapes with small aspect ratios (e.g., spheres and cubes). Conversely, the mean inverse intercept provides for an estimation of the *true three-dimensional thickness* of a thin membrane (e.g., oxide layers on particles), and is often applied to the estimation of thin, layered structures (e.g., pearlite, thickness of Widmanstätten  $\alpha$ -laths). Therefore, the mean linear

intercept is appropriate to provide an estimation of the equiaxed  $\alpha$  present in these microstructures. The result is that the mean size of the equiaxed  $\alpha$  particles is approximately equal to the mean linear intercept for random line segments in the  $\alpha+\beta$  processed Ti-6-4 microstructures. Indeed, for true spheres,  $D_{\text{sphere}} = 4/\pi d_{\text{mean}}$  [13]. However, for simplicity, and because the true three-dimensional shape is currently unknown, the mean size of the equiaxed  $\alpha$  particles is not multiplied by such a factor.

### 2.1.2 Volume Fraction of equiaxed $\alpha$ and total $\alpha$

After the preprocessing of the high resolution images, it is possible to use those images to perform an area fraction measurement to determine the volume fraction of the the various phases. Although there are two separate volume fractions of interest in this microstructure, that of the equiaxed  $\alpha$  phase and the total  $\alpha$  phase, the same methodology can be used to determine the volume fractions. This procedure follows the classical stereological procedures where the point fraction ( $P_P$ ), line fraction ( $L_L$ ), area fraction ( $A_A$ ) and volume fraction are equivalent. Practically, the area fraction is determined using the point count method, where the high resolution SEM micrographs, such as the one shown in Fig. 5(a), are essentially high density point grids, where every pixel is a point. This method can be automated, as was done for the analysis of the volume fraction of the equiaxed  $\alpha$  (see Fig. 5(c)) and the total volume fraction of  $\alpha$  (see Fig. 5(d)).

### 2.1.3 Thickness of Widmanstätten $\alpha$ -laths

For the determination of the thickness of the Widmanstätten  $\alpha$ -laths in transformed  $\beta$ , it is essential to subtract the equiaxed  $\alpha$  that has an identical contrast, and therefore, appears the same in the binary image. A Fovea Pro™ plug-in was used to perform this operation (see Fig. 5(e)). Subsequently, the same plug-in used to measure the size of the equiaxed  $\alpha$  particles was used to measure the *mean inverse intercept* length of the  $\alpha$ -laths. As described in section 2.1.1, this plug-in superimposes a grid of parallel lines on a binary image, rotates the grid by successive  $10^\circ$  increments to measure in all directions (see Fig. 5(f)), and reports both the mean linear intercept and the mean of the inverse of the intercepts. Given the three-dimensional shape of the Widmanstätten  $\alpha$ -laths (approaching a *layered* structure), the mean inverse intercept method is applied. The relation between the true thickness of an “infinite” plate of finite thickness (e.g.,  $\alpha$ -laths) was originally derived from the results of Gundersen [14] who was the first to apply the inverse of a lineal measurement to the problem of a thin membrane – i.e., a feature finite in one dimension and infinite in two dimensions. In this work, he demonstrated that while the probability distribution function of the intercept lengths was a complicated asymptotic shape, the probability distribution function of the inverse of the intercept lengths was a triangle, with the maximum occurring at  $\lambda^{-1} = 1/t_{\text{true}}$ . Therefore, as the mean  $(1/\lambda)_{\text{mean}}$  of a triangular probability distribution function is  $2/3$  of the max  $(1/t_{\text{true}})$ , the maximum can be estimated, and the true thickness can be calculated using the following relationship:

$$\text{thickness} = \left( \frac{1}{1.5(1/\lambda)_{\text{mean}}} \right)$$

Work now suggests that the probability density function for both the linear intercept and inverse linear intercept for the case of infinite plates of finite thickness varies from the original work of Gundersen [14] (*see Fig. 6 a-d*). Indeed, as can be shown, when two of the dimensions become finite (i.e., the case of a one-dimension infinite plate), the probability density functions will be modified to such a degree that the mean inverse intercept begins to deviate from the value of 0.67 (*see Fig. 7*). Although the probability distribution function of the inverse intercept no longer provides a mathematically simple, tractable solution, the determination of the mean inverse intercept  $((1/\lambda)_{mean})$  is still currently the most valid approach to estimating the true thickness when the ratio of the two dimensions is greater than  $\sim 20:1$ . It is expected that the use of mean inverse intercepts will break down for any case where the feature of interest does not have a ratio of the smallest dimension to the second smallest dimension of at least 1:20. While these observations do illustrate limitations with the mean inverse intercept method, it is still directly applicable for the case of Ti-based alloys. Additionally, it is interesting to note that the calculated mean inverse intercept for an infinite plate is 0.637, a value that is less than 5% different from the factor of 0.667 derived by Gundersen. It is acknowledged that this factor will change with particle shape. However, for consistency with previous work, and while new work aimed at modeling probability distribution functions for particles of finite shapes is currently underway, the thickness will be estimated by the above relationship, i.e., the best approximation currently available. To the best knowledge of the authors, this represents the first time where Gundersen's theory has been shown to be not applicable to all thin-membrane problems. Additional work is currently underway to develop a new set of methods for thin plates of various sizes, and will be the subject of future papers.

### **3 Results and Discussion**

While significant variations in both microstructure and properties were effected (Table 2), the primary focus of this paper is on the development of stereological procedures that can be used to describe accurately the average microstructural features for  $\alpha+\beta$  processed  $\alpha/\beta$  Ti-alloys, specifically Ti-6Al-4V. The following results and discussion will focus on the results of the stereological measurements, with particular emphasis on the statistics and quality of the measurements. To that end, four figures of merit will be considered. The first figure of merit will be a comparison of the analysis for each of the two identically heat-treated samples. It should be noted that, although microstructural variation between the two samples will be observed, there is often an associated variation in the properties, as little as  $\sim 7$  MPa (1 ksi) and as great as 42 MPa (6 ksi). The second figure of merit will be the standard deviation for the four micrographs that were recorded. The third figure of merit will be the Coefficient of the standard deviation in population ( $\sqrt{N}/N$ , %). The final figure of merit will be the coefficient of variation ( $\sigma/\mu \times 100$ , %). The results of these figures of merit are shown in Table 3.

Additionally, select microstructural features, as described by their mean, will be compared with both processing conditions and the overall yield properties. It should be noted that while the ultimate goal of such quantified microstructural features is the

population of a database to be used for the training and testing of Bayesian Neural Networks, the current database is not sufficiently large (i.e., only 17 sets of significant microstructural variations) to develop a robust neural network.

### 3.1 *Stereological Methods*

#### 3.1.1 *Volume Fraction of Phases*

In addition to being the oldest and most well understood stereological procedure, the determination of the volume fraction of a phase can also prove the most accurate under certain conditions. The primary conditions for the most accurate determination of volume fraction are that the plane of the image be random, and that the presence of a particular phase is equally likely at all points within a microstructure. Often, phase transformations satisfy the latter condition. Such is the case for the measurement of the total volume fraction  $\alpha$  in  $\alpha+\beta$  Ti-alloys. However, for those phases that preferentially form at certain locations of the microstructure, the measurement of volume fraction has as many uncertainties as other standard stereological procedures. For example, the presence of equiaxed  $\alpha$  is not homogeneously distributed throughout the microstructure. Indeed, the conditions required for the formation of equiaxed  $\alpha$ , namely  $\alpha$  at elevated temperatures and a concurrent strain, are not homogeneously distributed throughout the microstructure (high temperature  $\alpha$ ) or sample ( $\epsilon$ ). Therefore, one might expect low figures of merit for the volume fraction equiaxed  $\alpha$  as measured on 4 micrographs.

The quantified microstructures in this study confirm the expected outcome regarding the figures of merit for the determination of volume fraction of both total  $\alpha$  and equiaxed  $\alpha$ . The figures of merit indicating the data of the highest fidelity, including notably the lowest sample-to-sample variation (1.17%) and lowest coefficient of variation (0.98%), were those for the measurements of the volume fraction total  $\alpha$ . Conversely, the lowest figures of merit, including both the greatest sample-to-sample variation (11.2%) and greatest coefficient of variation (9.56%) were those for the measurements of the volume fraction equiaxed  $\alpha$ . As described above, the heterogeneous nature of equiaxed  $\alpha$  particle formation is the cause for the uncertainty. Therefore, it is expected that the figures of merit would improve with an increase in the sampling statistics (e.g., more micrographs) and the corresponding decrease in sample standard deviations.

#### 3.1.2 *Mean Equiaxed $\alpha$ particle size*

The stereological procedure for the determination of the mean equiaxed  $\alpha$  particle size results in reasonable figures of merit, as shown in Table 3. It is interesting to note that the three principal figures of merit (sample-to-sample variation coefficient, standard deviation of the population, and average coefficient of variation) are similar in magnitude (5.8%, 5.7%, and 4.8%, respectively). These are the second best figures of merit, after the volume fraction of total  $\alpha$ . It is expected that each of the figures of merit would decrease with an increase in sample population from the current population of 320-600 particles counted per sample (80-150 particles/micrograph, 4 micrographs). However, 10-20 micrographs would be required per sample to increase the total population to approximately 1600 particles, resulting in a decrease in the standard deviation of the population to  $\pm 2.5\%$ . Such sampling may or may not be required.

### 3.1.3 Thickness of Widmanstätten $\alpha$ -laths

Based on the figures of merit in Table 3, the method to determine the thickness of the Widmanstätten  $\alpha$ -laths is a relatively robust method. Indeed, it is suggested that the results obtained from 4 micrographs of an  $\alpha+\beta$  processed Ti microstructure are more accurate than those from a  $\beta$ -processed Ti microstructure. This expectation is the result of an improvement in the random sampling of different orientations that  $\alpha+\beta$  processed Ti-alloys afford, given the smaller regions of  $\beta$  regions of different orientations that exist prior to transformation. The figures of merit are misleading, given that the resolution of these micrographs is  $0.05 \mu\text{m} / \text{pixel}$ . Indeed, an adjustment of a single pixel to an average lath thickness ( $2/3 * \text{pixel}$ ) would result in a value that is identical to the sample-to-sample variation and average standard deviation that have been experimentally observed,  $0.03 \mu\text{m}$  and  $0.024 \mu\text{m}$ , respectively. By extension, for the thickness of the Widmanstätten  $\alpha$ -laths, it is expected that the coefficients of variations can not be less than  $\sim 5\text{-}7\%$ , as these are limited by the resolution of the microscope. Therefore, while it is acknowledged that the actual stereological pre-factor might change the accuracy of the calculations, the precision is only limited by the resolution in the micrographs. Similarly, it is important to compare the precision afforded by the high resolution SEM micrographs (500x in this case) to those of optical micrographs. Although the highest pixel resolution in optical microscopes is often  $0.1 \mu\text{m}$ , the highest practical resolution ( $0.2 \mu\text{m}$ ) is governed by the Rayleigh Criterion (the criterion for the minimum resolvable detail in an image) and occurs for an optimized optical microscope with a light wavelength of  $550 \text{ nm}$  and a numerical aperture of  $1.35$  to  $1.40$ . Clearly, the uncertainty afforded by using electron microscopy is significantly lower than what would be afforded using optical microscopy.

### 3.2 Correlation with processing

One benefit to the development of such databases is that it affords the possibility of investigating a variety of interdependencies, including, but not limited to, the influence of microstructure on properties and the influence of processing on microstructure. While the variation in thermomechanical processing is significant in this database, it is possible to keep most processing variables constant and investigate the influence of one processing variable on microstructure. For example, while one would expect the solution temperature and cooling rates to influence the size of the equiaxed  $\alpha$  particles and Widmanstätten  $\alpha$ -laths, it is beneficial to exercise the databases to demonstrate this. Figs. 8 (a-c) show the influence of isolated processing variables on such microstructural features. Fig. 8(a) shows that as the cooling rate from an aging temperature increases (both  $593^\circ\text{C}$  and  $704^\circ\text{C}$  shown), the thickness of the Widmanstätten  $\alpha$ -laths decreases. Fig. 8(b) shows that as the solution temperature decreases, the volume fraction of equiaxed  $\alpha$  increases and Fig. 8(c) shows that as the cooling rate from two separate temperatures decreases, the volume fraction of equiaxed  $\alpha$  increases. It is noted that these plots show the average and standard deviations of the stereological measurements for each of two identically processed samples. Thus, two discrete average data points and their uncertainties are provided for each value of a particular processing variable.

Interestingly, the relative uncertainties of the Widmanstätten  $\alpha$ -laths and equiaxed  $\alpha$ -particles are clearly observed when comparing Figs. 7(a) and 7(c), with the Widmanstätten  $\alpha$ -laths exhibiting a lower sample-to-sample variability and a lower uncertainty. These two trends are expected given the current understanding and models for the nucleation and growth of the equiaxed  $\alpha$  particles.

### 3.3 *Correlation with properties*

Figs. 9 (a-d) show the raw data correlations between the ultimate tensile strength and a particular microstructural variable. As can be observed, while it might be tempting to conclude that an increase in either equiaxed  $\alpha$  particle size or Widmanstätten  $\alpha$ -lath width results in a decrease in strength, the scatter in the data indicates that such trend plots do not allow a clear, unambiguous interpretation of the influence of a single microstructural variable and the resultant property, in this case, ultimate strength. The scatter in the plots is not an indication of the quality of the quantified microstructural feature. Rather, it is a direct consequence of the microstructural interdependencies. For example, consider the five samples highlighted in Table 4. Each sample has an equivalent ultimate tensile strength (within 7 MPa or 1 ksi), yet each of the four microstructural variables changes in a complicated, interrelated fashion. Such interdependencies require more robust modeling schemes, such as Bayesian Neural Networks, which require a larger database than that presented in this paper. These are the subject of ongoing work.

## 4 **Conclusions**

Standardized stereology procedures have been developed for the quantification of microstructural features in  $\alpha+\beta$  processed Ti-alloys, including the total volume fraction alpha, the volume fraction of equiaxed alpha, the mean size of the equiaxed  $\alpha$  particles, and an estimation for the thickness of the Widmanstätten  $\alpha$ -laths in the transformed  $\beta$  region. The development of these procedures, and the subsequent automation or semi-automation through software such as Adobe Photoshop™ and Fovea Pro™, have decreased or eliminated the bias (and associated errors) that occurs in more classical, fully manual stereology procedures. The uncertainties associated with each of the four procedures have been discussed.

### **Acknowledgements**

The development of the stereology procedures has occurred at the Center for the Accelerated Maturation of Materials at The Ohio State University, in collaboration with Dr. John Russ at North Carolina State University. The  $\alpha+\beta$  processed Ti-6Al-4V samples for this work have been provided from industrial partners under the Metals Affordability Initiative (MAI program) program (Air Force Office of Scientific Research). The analysis of uncertainties and sources of error has occurred as part of the further development of the stereology procedures presented in this paper and has been funded by the Office of Naval Research, program # 2626753 Direct-3-Dimensional (D-3D), Dr. Julie Christodoulou, program officer.

## References:

1. G. Lütjering: *Proceedings, 9<sup>th</sup> World Titanium Conference*, China, 1998, pp. 1-19.
2. R. Boyer, G. Welsch, E.W. Collings: *Materials Properties Handbook: Titanium Alloys*, ASM International, Materials Park, OH, 1994.
3. P. A. Blenkinshop, W.J. Evans, H. M. Flower, eds.: *Titanium '95: Science and Technology, Proceedings of the 8<sup>th</sup> World Conference on Titanium*, The Institute of Materials, London, UK, 1996.
4. G. Lütjering: *Materials Science & Engineering A*, vol. 243, 1998, pp. 32-45.
5. G. Lütjering: *Materials Science and Engineering A*, 1999, vol. 263, pp. 117-126.
6. D.J.C. MacKay: PhD Thesis, 1992, California Inst. Of Tech., Pasadena, CA.
7. <http://www.inference.phy.cam.ac.uk/mackay/>
8. D.J.C. Mackay: *Neural Computation*, vol. 4(3), 1992, pp 448-472.
9. J. Tiley, T. Searles, E. Lee, S. Kar, R. Banerjee, J.C. Russ, and H.L. Fraser: *Mater. Sci. Eng. A*, 2004, vol. 372, pp. 191-198.
10. S. Kar, T. Searles, E. Lee, G.B. Viswanathan, J. Tiley, R. Banerjee, and H.L. Fraser: *Metallurgical and Materials Transactions A*, vol. 37A (3), 2006, pp 559-566.
11. T. Searles, J. Tiley, A. Tanner, R. Williams, B. Rollins, E. Lee, S. Kar, R. Banerjee, and H.L. Fraser: *Measurement Science & Technology*, vol 16 (1), 2005, pp 60-69.
12. P.C., Collins, H.L. Fraser - In final preparation - to be published.
13. J. Russ, R. Dehoff, *Practical Stereology*, Kluwar Academic Publishers/Plenum Publishers, Dordrecht/New York, 2000.
14. HJG Gundersen, EB Jenson, R Osterby, "Distribution of membrane thickness determined by lineal analysis", *J Microscopy*, 1978, 113:27.

## Figure Captions:

Fig. 1: (a) basketweave microstructures from  $\beta$ -processed Ti-6Al-4V and (b) equiaxed microstructures from  $\alpha+\beta$  processed Ti-6Al-4V.

Fig. 2: (a) Example micrograph (b) histogram from alpha region with channeling contrast (c) histogram from alpha region without channeling contrast (d) histogram from complete microstructure and (e) thresholded image

Fig. 3: (a) small equiaxed  $\alpha$ , low volume fraction (b) large equiaxed  $\alpha$ , small volume fraction (c) large equiaxed  $\alpha$ , large volume fraction

Fig. 4: (a) Original backscattered electron micrograph (b) original automated identification of equiaxed  $\alpha$  illustrating over-identification (c) manual refinement of automated identification and (d) manual separation of clusters of equiaxed  $\alpha$  particles

Fig. 5: Original image (a) and representative processed images for the measurement of (b) equiaxed  $\alpha$  particle size (c) volume fraction of equiaxed  $\alpha$  (d) total volume fraction of  $\alpha$  and (e) isolation and (f) thickness measurement of the Widmanstätten  $\alpha$ -laths.

Fig. 6: Probability distribution functions vs the intercept length for (a) Gundersen's derivation of membranes (b) distribution through an infinite plate of finite thickness (c) comparison of the two; and probability distribution functions vs. the inverse intercept length for (d) Gundersen's derivation of membranes (e) infinite plates of finite thickness and (f) a comparison of both.

Fig. 7: Calculated mean inverse intercept from the probability density function of inverse intercept for 1-D infinite plates where the two other dimensions (width and thickness) are given by their ratio.

Fig. 8: Influence of processing variables on selected microstructural features, including (a) Widmanstätten  $\alpha$ -lath thickness vs. cooling rate from the aging temperature for samples subjected to a total strain of 80% (b) solution temperature vs. the volume fraction of equiaxed  $\alpha$  for samples subjected to a total strain of 40% and cooled at 3.7°C/sec and (c) the volume fraction of equiaxed  $\alpha$  vs. the cooling rate from the aging temperature for samples subjected to a total strain of 80%.

Fig. 9: Raw data scatter plots for the UTS vs. the four microstructural variables quantified in  $\alpha/\beta$  processed  $\alpha/\beta$  Ti alloys (here Ti-6Al-4V).

#### **List of Tables:**

Table 1: Full details of thermomechanical processing.

Table 2: Ranges of microstructural variables as determined using stereology and the ranges of properties in the developed database.

Table 3: Figures of Merit.

Table 4: Samples with similar properties but different microstructural features.

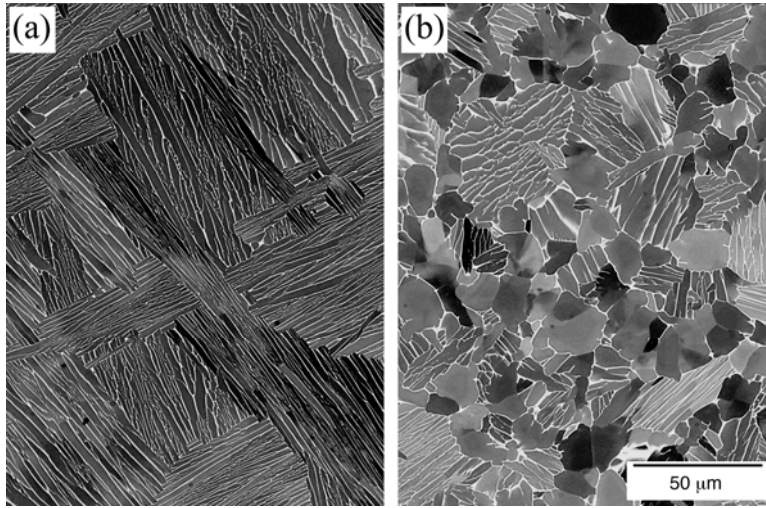


Fig. 1: (a) basketweave microstructures from  $\beta$ -processed Ti-6Al-4V and (b) equiaxed microstructures from  $\alpha+\beta$  processed Ti-6Al-4V.

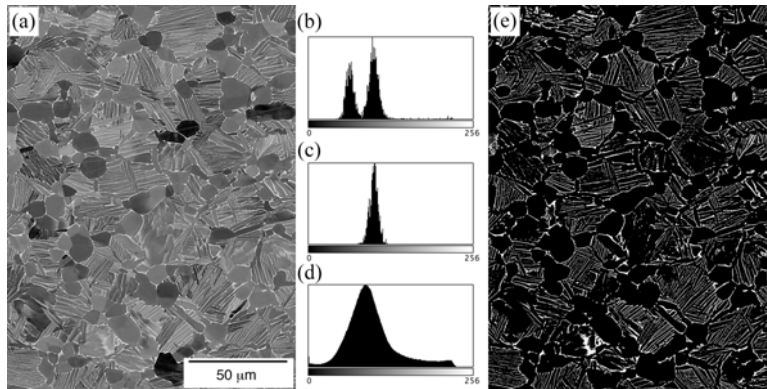


Fig. 2: (a) Example micrograph (b) histogram from alpha region with channeling contrast (c) histogram from alpha region without channeling contrast (d) histogram from complete microstructure and (e) thresholded image

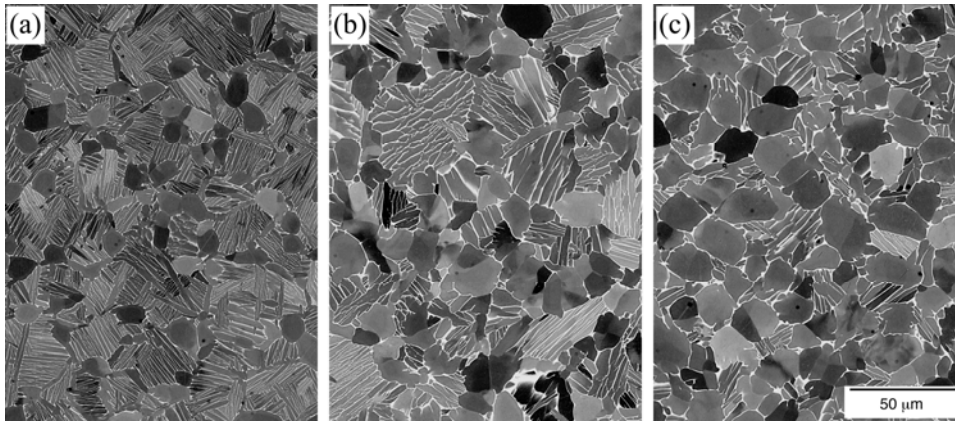


Fig. 3: (a) small equiaxed  $\alpha$ , low volume fraction (b) large equiaxed  $\alpha$ , small volume fraction (c) large equiaxed  $\alpha$ , large volume fraction

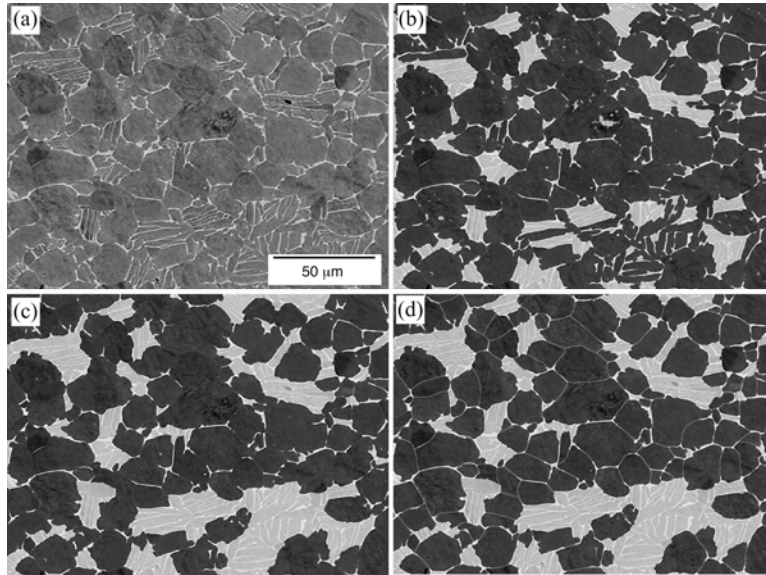


Fig. 4: (a) Original backscattered electron micrograph (b) original automated identification of equiaxed  $\alpha$  illustrating over-identification (c) manual refinement of automated identification and (d) manual separation of clusters of equiaxed  $\alpha$  particles

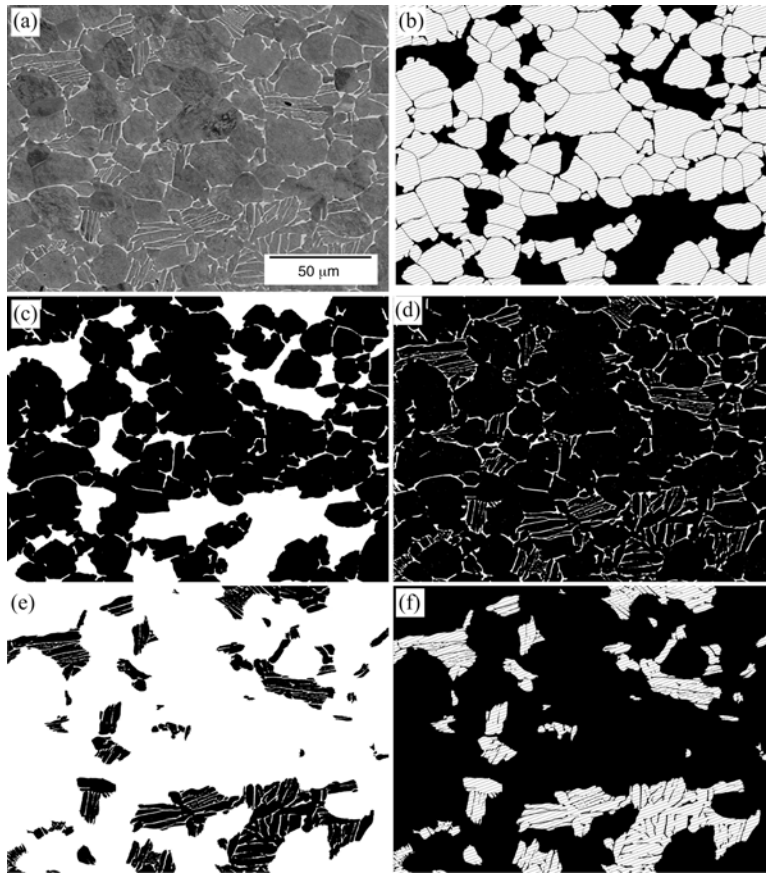


Fig. 5: Original image (a) and representative processed images for the measurement of (b) equiaxed  $\alpha$  particle size (c) volume fraction of equiaxed  $\alpha$  (d) total volume fraction of  $\alpha$  and (e) isolation and (f) thickness measurement of the Widmanstätten  $\alpha$ -laths.

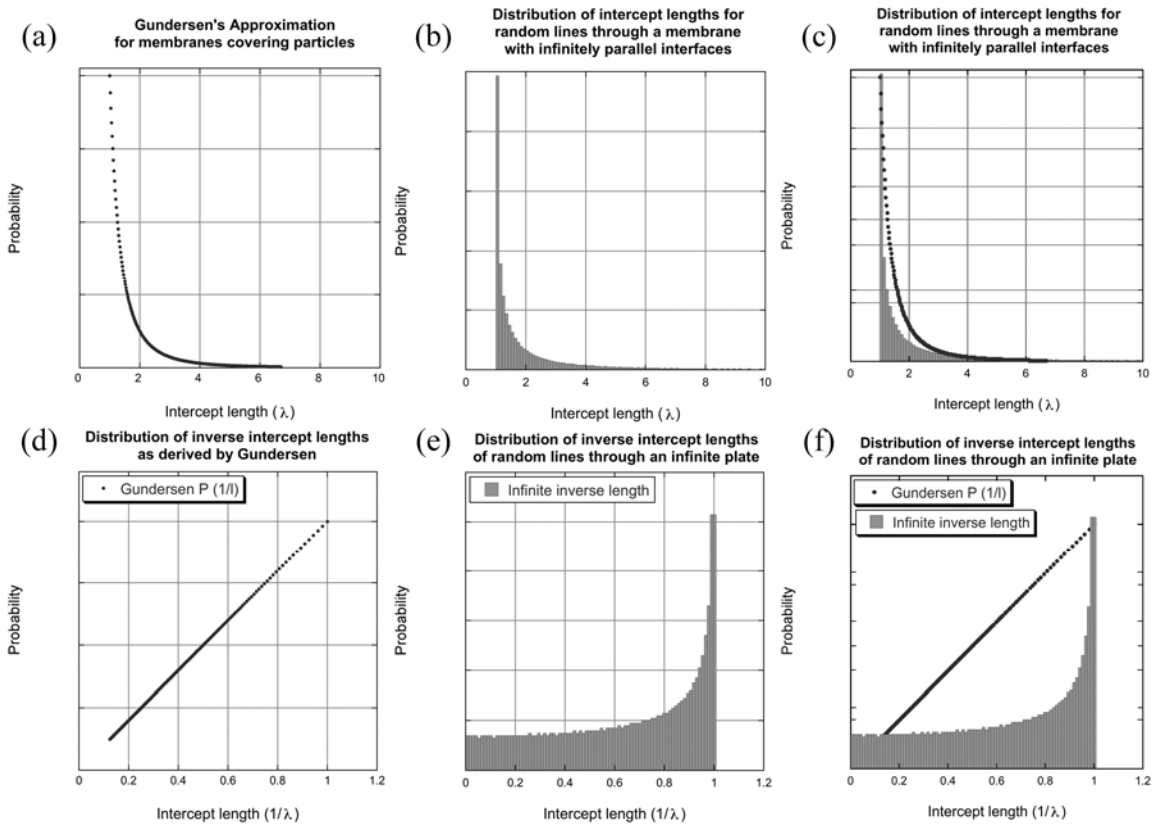


Fig. 6: Probability distribution functions vs the intercept length for (a) Gundersen's derivation of membranes (b) distribution through an infinite plate of finite thickness (c) comparison of the two; and probability distribution functions vs. the inverse intercept length for (d) Gundersen's derivation of membranes (e) infinite plates of finite thickness and (f) a comparison of both.

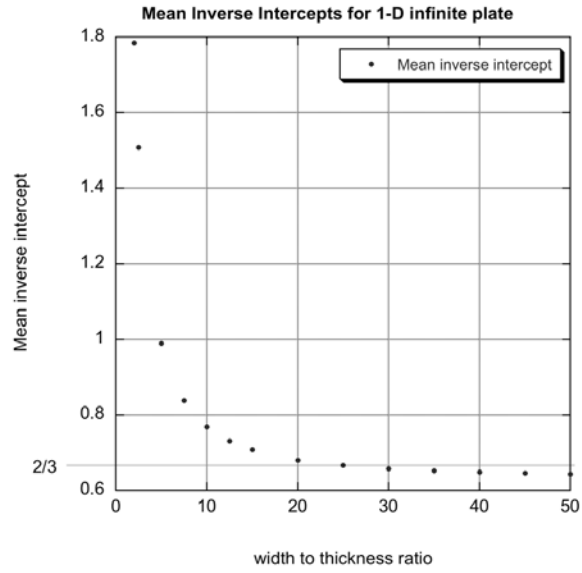


Fig. 7: Calculated mean inverse intercept from the probability density function of inverse intercept for 1-D infinite plates where the two other dimensions (width and thickness) are given by their ratio.

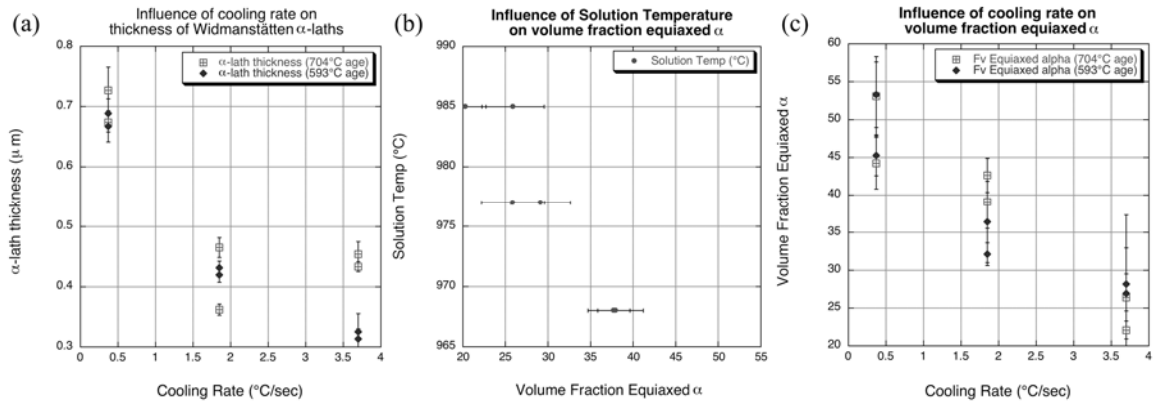


Fig. 8: Influence of processing variables on selected microstructural features, including (a) Widmanstätten  $\alpha$ -lath thickness vs. cooling rate from the aging temperature for samples subjected to a total strain of 80% (b) solution temperature vs. the volume fraction of equiaxed  $\alpha$  for samples subjected to a total strain of 40% and cooled at 3.7 $^{\circ}\text{C}/\text{sec}$  and (c) the volume fraction of equiaxed  $\alpha$  vs. the cooling rate from the aging temperature for samples subjected to a total strain of 80%.

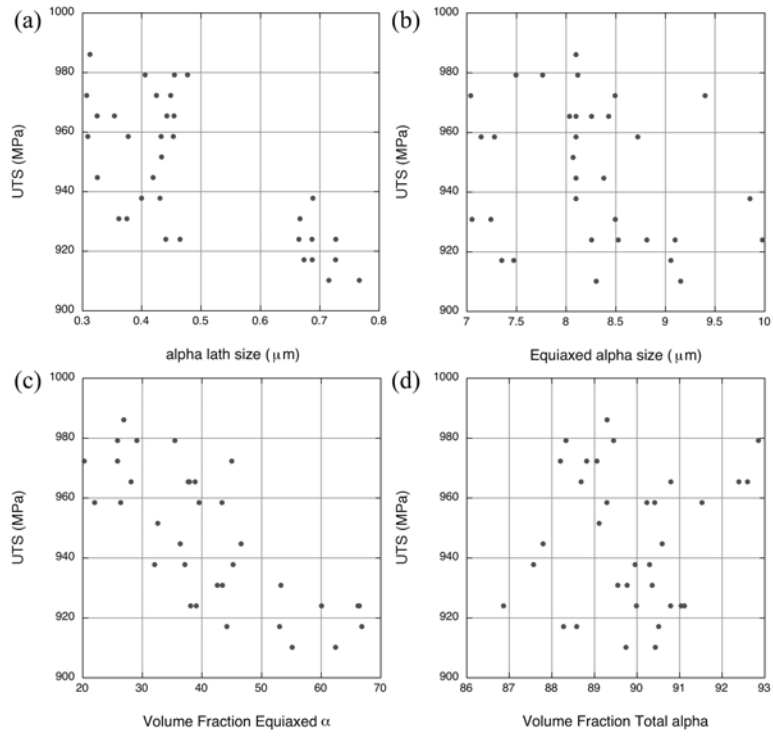


Fig. 9: Raw data scatter plots for the UTS vs. the four microstructural variables quantified in  $\alpha/\beta$  processed  $\alpha/\beta$  Ti alloys (here Ti-6Al-4V).